Deoxyribonucleic Acid as a Universal Electrolyte for Bio-Friendly Light-Emitting Electrochemical Cells

Serpil Tekoglu,* Martin Held, Markus Bender, Guan Ni Yeo, Andreas Kretzschmar, Manuel Hamburger, Jan Freudenberg, Sebastian Beck, Uwe H. F. Bunz, and Gerardo Hernandez-Sosa*

In the search for bio and eco-friendly light sources, light-emitting electrochemical cells (LECs) are promising candidates for the implementation of biomaterials in their device architecture thanks to their low fabrication complexity and wide range of potential technological applications. In this work, the use of the DNA derivative DNA-cetyltrimethylammonium (DNA-CTMA) is introduced as the ion-solvating component of the solid polymer electrolyte (SPE) in the active layer of solution-processed LECs. The focus is particularly on the investigation of its electrochemical and ionic conductivity properties demonstrating its suitability for device fabrication and correlation with thin film morphology. Furthermore, upon blending with the commercially available emissive polymer Super Yellow, the structure property relationship between the microstructure and the ionic conductivity is investigated and yields an optimized LEC performance. The large electrochemical stability window of DNA-CTMA enables a stable device performance for a variety of emitters covering the complete visible spectral range, thus highlighting the universal character of this naturally sourced SPE.

1. Introduction

The utilization of biodegradable and biocompatible materials as active and passive components for optoelectronic devices has recently attracted significant attention.[1–6] These efforts are motivated by the need in developing more sustainable consumer electronics and their potential use in bio-electronic and wearable applications.[7–11] On the one hand, biodegradable electronics could help to counteract the rapid increase in the global volume of electronic waste of which only an estimated 15% is fully recycled.[12,13] On the other hand, biocompatible

devices will contribute to develop novel medical treatments in the field of optogenetics or bioresorbable implants and assist in the understanding of biological processes.[10,14,15]

In the field of electroluminescent devices, organic light-emitting electrochemical cells (LECs) have emerged as a high performance technology with reduced processing complexity and simplified device architecture compared to that of organic light-emitting diodes (OLEDs).[16,17] Furthermore, its single-layer nature comprising an electrolyte:semiconductor mixture renders it particularly well-suited for the implementation of bio-friendly materials.[18–21] Generally, solid polymer electrolytes (SPEs) have been a key component in the development of current state-of-the-art LECs.[22–27] In SPEs, the ion-solvating polymer chain serves as the scaffold medium for mobile ions enabling the dynamic creation of a p-i-n junction. Optimizing parameters, such as i) ionic concentration, ii) electrochemical stability, and iii) phase separation with the emissive materials, is a crucial task for maximizing device performance.[27] Our recent work has demonstrated the use of biodegradable synthetic polymers such as polycaprolactone, poly(lactic-co-glycolic acid), and poly(caprolactone-co-trimethylene carbonate) in the SPE of solution-processed LECs as a route to investigate the parameter space and processing steps necessary to fabricate bio- and eco-friendly devices.[18–21] In turn, bio-based polymers represent an alternative approach to be

Dr. S. Tekoglu,[+] Dr. M. Held, G. N. Yeo, Dr. G. Hernandez-Sosa
Light Technology Institute
Karlsruhe Institute of Technology
Engesserstr. 13, Karlsruhe 76131, Germany
E-mail: serpil.tekoglu@jku.at; gerardo.sosa@kit.edu

The ORCID identification number(s) for the author(s) of this article can be found under https://doi.org/10.1002/adsu.202000203.

[+]Present address: Linz Institute for Organic Solar Cells (LIOS), Physical Chemistry, Johannes Kepler University Linz, Altenbergerstraße 69, Linz 4040, Austria

Dr. S. Tekoglu,[+] Dr. M. Held, G. N. Yeo, Dr. M. Hamburger, Dr. S. Beck, Dr. G. Hernandez-Sosa
InnovationLab
Speyerer Str. 4, Heidelberg 69115, Germany

Dr. M. Bender, Dr. A. Kretzschmar, Dr. M. Hamburger, Dr. J. Freudenberg, Prof. U. H. F. Bunz
Organisch-Chemisches Institut
Ruprecht-Karls-Universität
Im Neuenheimer Feld 270, Heidelberg 69120, Germany

Dr. S. Beck
Kirchhoff-Institut für Physik
Ruprecht-Karls-Universität
Im Neuenheimer Feld 227, Heidelberg 69120, Germany

Prof. U. H. F. Bunz
Centre for Advanced Materials
Ruprecht-Karls-Universität Heidelberg
Im Neuenheimer Feld 225, Heidelberg 69120, Germany

**ADVANCED
SCIENCE NEWS**

www.advancedsciencenews.com

**ADVANCED
SUSTAINABLE
SYSTEMS**

www.advsustainsys.com

explored as they have evolved in biological systems concomitant with the appropriate life-cycles.

DNA is a natural polyelectrolyte that combines ionic conductivity and the properties of soft plastic materials.[28] Its high transparency, high thermal stability, and thin film processability, in addition to its natural abundance and renewability, have diverted the attention of researchers toward the use of DNA in the fields of photonics and optoelectronics.[29,30] Furthermore, the complex formation of DNA with the surfactant cetyltrimethylammonium (CTMA) chloride via simple ion-exchange reaction renders the adduct DNA-CTMA soluble in alcohols, opening up its processability for a vast range of applications.[30,31] DNA-CTMA has been employed in non-linear optics,[30,32] lasers,[33,34] as well as the gate dielectric of organic transistors,[35,36] and memory elements.[37] In OLEDs, DNA has been utilized as a hole transport and electron blocking layer[38–40] and as a host for luminophores in the emissive layer.[41,42] The suitability as a host-material was even extended from electro- to chemiluminescence.[43] The electrochemical properties of DNA and DNA-CTMA gel polymer electrolytes led to the application in ion-conducting membranes in electrochromic devices,[44,45] lithium-ion batteries[46] and dye-sensitized solar cells.[47] Despite these exciting attributes provided by DNA in optoelectronics, no application of DNA in LECs has been comprehensively investigated.

In this work, we focus particularly on DNA-CTMA as the ion-solvating component of the SPE in the active layer of solution-processed LECs. Morphological studies on different length scales complement the electrical and electrochemical characterization of the DNA-CTMA-based SPE and its blend with the commercially available emissive polymer Super Yellow (SY), which demonstrates LEC devices with promising performance. The outstanding electrochemical properties of DNA-CTMA, particularly its wide electrochemical window, enabled the expansion to a pool of eight emitters covering the entire visible spectrum, rendering DNA-CTMA a universal SPE for visible light emission. These devices emphasize the potential toward further development of bio-LECs with DNA-based electrolytes, which could constitute the future light sources in disposable, especially biodegradable, and bio-compatible electronic applications.

2. Results and Discussion

2.1. DNA-CTMA for SPEs

The double helical molecular structure of DNA is composed of a negatively charged phosphate-deoxyribose backbone, linking nucleobases and H^+ or Na^+ cations to balance the charges.[48] Due to the charged backbone and complex structure, DNA is an anionic polyelectrolyte with a high molecular weight, in which counter ions can move freely.[28] This fundamental property qualifies DNA to be applied in combination with salts as SPEs in LECs. However, as DNA is insoluble in organic solvents, the device fabrication from aqueous solutions limits the choice of co-dissolved emitting polymers to compounds with water-solubilizing side-chains. Our results of combining the water-soluble derivative of poly(para-phenylene) with DNA and the salt potassium triflate (KCF_3SO_3) in blue-emitting LECs revealed a fundamental dilemma for electrolyte films which

were deposited from aqueous solutions (details in Section S1, Supporting Information): Increased drying time and temperature of the SPE layer decreased the ionic conductivity of the electrolyte and thus the performance of the LEC. The presence of residual water resulted in extremely short lifetimes of the LECs due to device degradation. To prevent this issue, an ion exchange of sodium cations with the cationic surfactant CTMA was conducted and confirmed by Fourier-transform infrared spectroscopy (details in Section S2, Supporting Information). The resulting DNA-CTMA adduct is soluble in alcohols[30] and can thus be solution-processed together with common organic emitters (**Figure 1**a).

In order for DNA-CTMA to serve as an SPE in LECs, its fundamental electrochemical properties were investigated. The electrochemical stability window of an SPE defines the voltages above which undesired electrochemical reactions take place during device operation.[23,24] These may involve the salt, the polymer but also the solvent. The cyclic voltammogram, after covering the working electrode with a DNA-CTMA film (in a tetrabutylammonium tetrafluoroborate ($TBABF_4$) solution), does not reveal additional redox peaks compared to a $TBABF_4$ solution (Figure 1b). The oxidation onset remains at around 1.5 V and reduction onset at around −2.25 V (both versus Fc/Fc⁺). A cyclic voltammogram of a film with a 1:1 blend DNA-CTMA:$TBABF_4$ reveals nearly the same redox onsets. Previously, LUMO and HOMO levels of DNA-CTMA have been reported to be −0.9 and −5.6 eV, respectively.[37–40,42] The corresponding reduction onset of −3.9 V versus Fc/Fc⁺ is located outside the recorded peaks, whereas the corresponding oxidation onset of +0.8 V seems to be kinetically inhibited. Thus, for kinetic reasons, DNA-CTMA-based SPEs may provide an electrochemical stability window from −2.25 to 1.5 V versus Fc/Fc⁺.

Within the electrochemical stability window, the effective concentration of ions is greatly dependent on the SPE's composition, and so is the ability to electrochemically dope the emitter during LEC operation. The ionic conductivities of DNA-CTMA:$TBABF_4$ blends with varying salt ratios were obtained using impedance spectroscopy and suitable equivalent circuit models (details in Section S3, Supporting Information). The mean value of the ionic conductivity of pure DNA-CTMA was found to be $5.5 \cdot 10^{-8}$ S cm⁻¹ (Figure 1c), which is in a good agreement with the previously published data for DNA-CTMA membranes at 28.7 °C ($3.9 \cdot 10^{-8}$ S cm⁻¹).[29]

The ionic conductivity of the DNA-CTMA:$TBABF_4$ films decreases from pure DNA-CTMA with increasing salt ratio. Initially, an increasing salt ratio in the polymer electrolyte may trigger the formation of ion pairs and ion aggregates, which may decrease the effective concentration of dissociated ions and reduce the overall ionic conductivity of the SPE. A further rise of the salt concentration may overcome this trapping mechanism, as the experimental data shows for salt ratios above (1:0.5). Coherently, the highest ionic conductivity with salt amounts to $2.6 \cdot 10^{-9}$ S cm⁻¹ at a DNA-CTMA:$TBABF_4$ ratio of (1:1).

The white light interferometry images of the SPE films reveal a salt ratio dependent surface topography and film morphology at the micrometer scale (**Figure 2**a). While the pure DNA-CTMA film presents an amorphous morphology, the addition of small amounts of $TBABF_4$ creates an abundance of clusters that increase in size and number up to a ratio of (1:0.07).
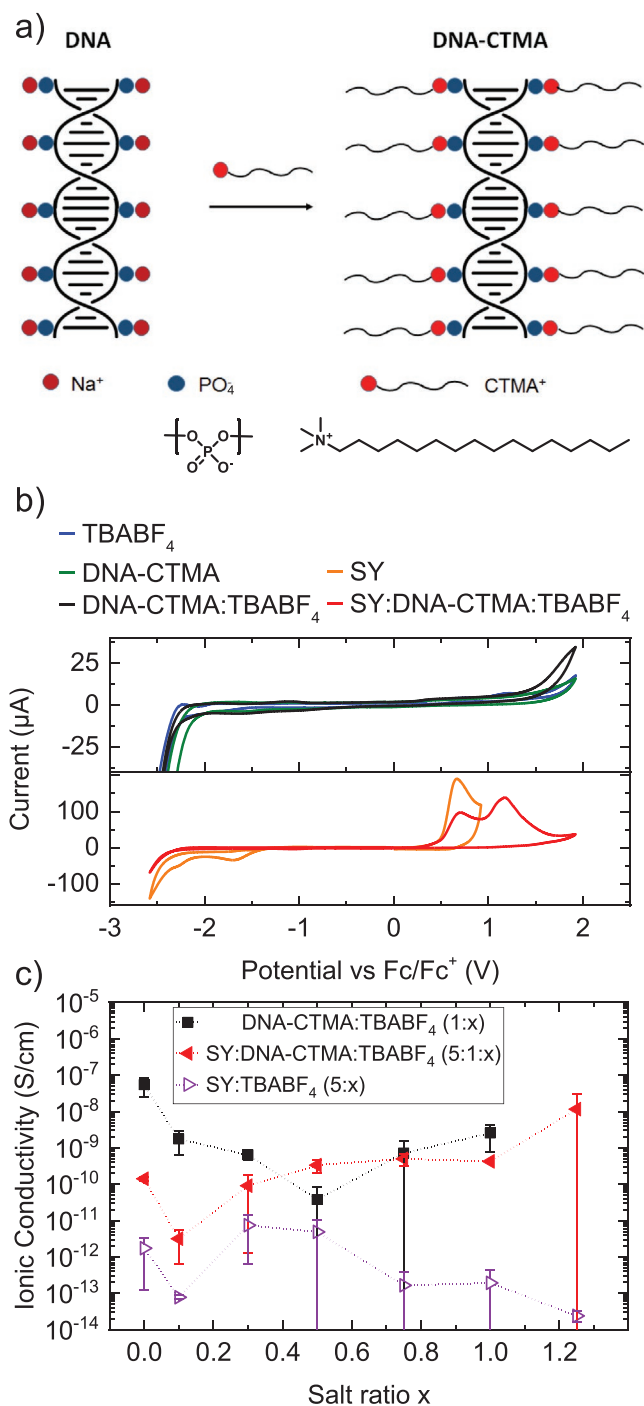
Figure 1. Electrochemical properties of DNA-CTMA. a) Schematic modification of DNA with the CTMA surfactant. b) Cyclic voltammograms of a TBABF$_4$ solution compared to thin-films of DNA-CTMA, SY, and the blends DNA-CTMA:TBABF$_4$ (1:1) and SY:DNA-CTMA:TBABF$_4$ (5:1:1). Solvent: acetonitrile, scan rate: 0.05 V s^{-1}. c) Ionic conductivity of DNA-CTMA:TBABF$_4$, SY:DNA-CTMA:TBABF$_4$, and SY:TBABF$_4$ blends with different TBABF$_4$ salt concentrations.

Further increasing the salt ratio disperses the precipitates and reduces their size. The (1:0.1) film emphasizes the aggregation tendency and exhibits the highest root-mean-square roughness values. At a salt ratio of (1:0.12) a transition from precipitates toward grain boundaries occurs, which becomes gradually more prominent at (1:0.18) and (1:0.3). This trend continues by the appearance of precipitates within the grains in excess of salt, as indicated by the expanded micrograph in Figure 2a at a ratio of (1:1.25). Figure 2b schematically illustrates the transition from disordered precipitates to grain boundaries to grains with salt precipitates.

The salt aggregation and grain boundary formation may explain the overall lower ionic conductivity of the DNA-CTMA:TBABF$_4$ blends, whereas the reduction of the size of the precipitates correlates with the rise in ionic conductivity of the blends. Further, the presence of these precipitates and grain boundaries were reflected in the impedance spectra, which are successfully modeled with a grain boundary equivalent circuit (details in Section S3, Supporting Information).
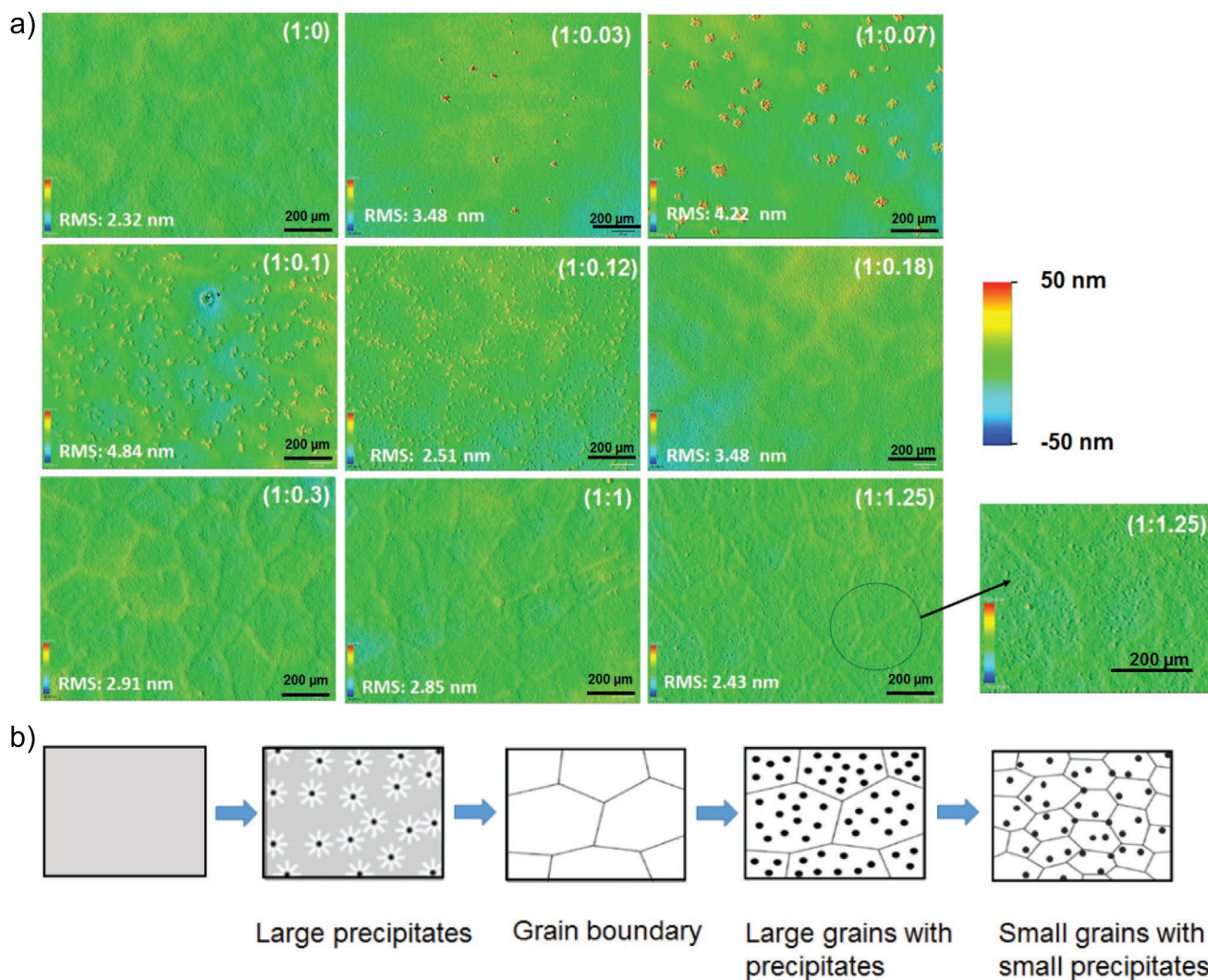
2.2. DNA-CTMA Based SPEs for LECs

In an LEC the SPE is blended in solution with an organic semiconductor before deposition, in this case the yellow-emitting polymer SY. DNA-CTMA is soluble in alcohols, which does not dissolve SY. Therefore SY, DNA-CTMA, and TBABF$_4$ were dissolved in a 2:1 mixture of chloroform:butanol. Employing solvent mixtures aids in overcoming the main disadvantage of DNA-CTMA: Their low solubility in non-alcoholic solvents. The SY:DNA-CTMA ratio is fixed at (5:1) and the salt ratio is altered in the blend.

For a stable operation of LECs the p- and n-doping state of the semiconductor should remain within the electrochemical stability window of the SPE to eliminate irreversible electrochemical side reactions.[23,24] Solid polyelectrolytes with larger electrochemical stability windows have been reported to improve the lifetime of LECs.[25–27] The electrochemical reduction and oxidation onsets of pure SY are measured at −2.1 and +0.4 V versus Fc/Fc$^+$ (Figure 1b), respectively, matching previous reports.[25,49] The small peak at −1.5 V is irreversible and does not correlate to any previously described LUMO values. The blend of SY:DNA-CTMA:TBABF$_4$ exhibits the same oxidation onset of SY, whereas the minor peak at −1.5 V disappears, likely due to kinetic effects. In essence, SY does not exceed the redox potentials of the DNA-CTMA:TBABF$_4$ electrolyte and reliable electrochemical doping occurs in the active layer blend during device operation.

Blending SY with DNA-CTMA at a ratio of (5:1) dramatically reduced the ionic conductivity σ_i by more than two orders of magnitude to an average of 1.4·10^{-10} S cm^{-1}, compared to 5.5·10^{-8} S cm^{-1} for pure DNA-CTMA (Figure 1c). This can clearly be attributed to the high content of SY, which contains no ions, and exhibits a very low σ_i = 1.7·10^{-12} S cm^{-1}. Adding salt to the SY:DNA-CTMA blend steadily increases σ_i to comparable levels of the DNA-CTMA:TBABF$_4$ samples. In contrast to the latter, no trapping mechanism at low salt concentration was observable.

The white light interferometry images confirm the absence of a trapping mechanism for all salt ratios between (5:1:0) and (5:1:1.25) by presenting a uniform topography without precipitations or grain boundaries (Figure S4.1, Supporting Information). Likely, the presence of SY aided in the dispersion of ions. Still, the impedance spectra of these samples required a grain boundary equivalent circuit model, which can be attributed to

**ADVANCED
SCIENCE NEWS**

www.advancedsciencenews.com

**ADVANCED
SUSTAINABLE
SYSTEMS**

www.advsustainsys.com

Figure 2. a) Interferometric topography images of DNA-CTMA:TBABF$_4$ (1:x) films on glass, including the root-mean-square roughness (RMS) and a magnification of the (1:1.25) film. b) Schematic description of aggregation and grain formation in the thin films.

two parallel ion conduction mechanisms of DNA-CTMA and SY, since the chemical interactions between non-ionic semiconducting polymers and ionic biopolymers such as DNA or proteins are relatively small (details in Section S3, Supporting Information).[50]

In polymer LECs the active layer may encounter phase separation between the emitting polymer and the ion-solvating polymer or polyelectrolyte, which drastically decreases the device performance.[51,52] This phenomenon originates in the polarity mismatch between the non-polar semiconducting polymer and the polar ion-solvating polymer or polyelectrolyte, for example, for PMMA:SY LECs.[52] Photoluminescence microscopy images of 5:1 blends of SY:DNA-CTMA do not show a complete phase separation but merely a SY-richer (brighter) and SY-poorer (darker) phase (Figure S4.2, Supporting Information). The weak contrast between these phases however vouches for a well-mixed active layer.

After having unveiled a homogeneous mixing of the polymers and salt, as well as the emitting and electrolyte polymer,

the morphology and aggregation tendency of SY:DNA-CTMA:TBABF$_4$ blends is further investigated on the nanoscale. Atomic force microscopy topographic images of these blends exhibit a homogeneous intermixing of all components, regardless of the salt content (Figure S4.3, Supporting Information). The magnitude of the film roughness compared to the film thickness resulted in the formation of short cuts which reduced fabrication yield of working devices.

The homogeneous micro- and nanostructure of the SY:DNA-CTMA:TBABF$_4$ blends renders these films as suitable active layers for LECs by sandwiching them between Ag and ITO (**Figure 3**a). A homogeneous light output over the entire pixel area was recorded for all samples, independent of the TBABF$_4$ content (Figure 3b and Figure S4.4a, Supporting Information). The electroluminescence spectrum and the Commission Internationale de l'Eclairage (CIE) coordinates of the LECs with DNA-CTMA are identical to a reference OLED with SY (Figure S4.4b,c, Supporting Information). Thus, DNA-CTMA does not optically interact with SY in operation. As DNA-CTMA
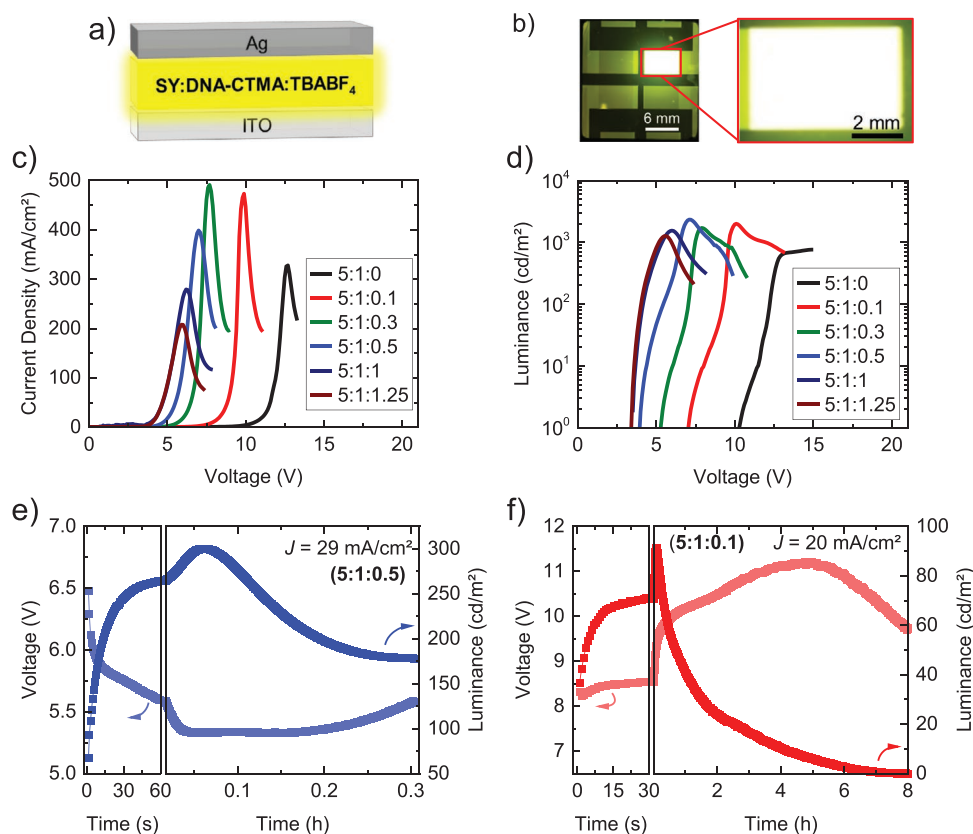
Figure 3. SY:DNA-CTMA:TBABF$_4$ LECs. a) Device architecture. b) Photograph of the 0.24 cm^2 LEC pixel under operation. c) Current density–voltage and d) luminance–voltage characteristics. Scan rate 0.09 V s^{-1}. e) Steady-state (time in s) and lifetime (time in h) characteristics for the w/w ratio of (5:1:0.5) at 29 mA cm^{-2} and f) for (5:1:0.1) at 20 mA cm^{-2}.

is transparent in the visible region, the device color is determined by the emitter.

However, varying the salt ratio in these blends affected their optoelectronic performance in luminance-current density-voltage (LIV) sweeps (Figure 3c). A higher number of ionic species, causing higher ionic conductivity, steadily reduced the turn-on voltage (voltage at 1 cd) from 10.7 ± 0.28 V for (5:1:0) to 3.36 ± 0.07 V for (5:1:1.25) (**Table 1**). The maximum luminance ranged within 1500–2000 cd m^{-2} and peaked at 2332 cd m^{-2} for the (5:1:0.5) SY:DNA-CTMA:TBABF$_4$ blend (Figure 3d). The highest efficiency at low luminance was obtained for the ratio of (5:1:1.25), whereas (5:1:0.5) was more efficient at

higher light intensity (Figure S4.4d, Supporting Information). The dependence of the maximum luminance and efficiency on the salt content can merely be rationalized with competing effects of increased electrochemical doping and doping-induced quenching that lead to a peak performance at a certain salt concentration.

In addition to voltage sweeps, time-dependent measurements were conducted on SY:DNA-CTMA:TBABF$_4$ LECs. During the galvanostatic operation at a fixed current, an asymptotical decrease in voltage and increase in luminance over time indicates the formation of ohmic contacts due to the in situ formed electrical double layers promoting electrochemical doping and reveals the steady-state performance of LECs,[53,54] as can be observed in the first 60 s in Figure 3e,f. The reduction of the luminance to 50% of the steady-state value over time defines the lifetime, at constant current. Samples with an intermediate salt ratio (5:1:0.5) have a shorter lifetime of 0.3 h at 29 mA cm^{-2} (Figure 3e), while lower salt ratios (5:1:0.1) increased the lifetime to around 1 h at a constant current of 20 mA cm^{-2} (Figure 3f). As previously reported, LECs comprising a larger amount of salt exhibit faster turn-on time but a shorter lifetime.[55,56] Furthermore, a higher current density fuels the magnitude of undesired side reactions, which thereupon results in a shorter operational lifetime.[24,57]

The composition of the LEC's active layer should therefore be tuned to the specification of the LEC's application. Previous

Table 1. Device characteristics of SY:DNA-CTMA:TBABF$_4$ LECs.

SY:CTMA:TBABF$_4$	V_{on}[a] [V]	L_{max}[b] [cd m^{-2}]	Eff$_{max}$[c] [cd A^{-1}]
5:1:0	10.7 ± 0.28	816 ± 85	0.42 ± 0.2
5:1:0.1	7.02 ± 0.35	2179 ± 283	0.56 ± 0.13
5:1:0.3	5.01 ± 0.4	1755 ± 421	0.57 ± 0.07
5:1:0.5	4.08 ± 0.15	2294 ± 140	0.64 ± 0.06
5:1:1	3.45 ± 0.07	1717 ± 311	0.96 ± 0.22
5:1:1.25	3.36 ± 0.07	1649 ± 395	1.08 ± 0.06

[a]Turn-on voltage at 1 cd m^{-2}; [b]Maximum luminance; [c]Maximum current efficiency at LIV sweep. Values obtained by averaging over at least four pixels.

work revealed that doping-induced quenching phenomena require a focus on either high efficiency or high brightness.[58] Contrary to this previous report, the DNA-CTMA-based LECs require high salt ratios for high efficiency, while high brightness requires intermediate salt concentrations. This might be explained by a higher doping efficiency of the DNA-CTMA SPE, leading to a strong reduction in current density and thus an efficiency increase. The efficiency roll-off will likely appear at even higher salt content. In coherence with literature, long lifetimes require low salt concentrations for this SPE system (Table 1).[27]

In order to distinguish the effect of DNA-CTMA on the performance of the LECs, SY:TBABF$_4$ reference LECs were also fabricated. The SY:TBABF$_4$ films showed a homogeneous distribution of the surface morphology without any observable grain boundaries (Figure S5.1, Supporting Information), probably due to the better intermixing of salt and SY compared to salt and DNA-CTMA. This improved intermixing will likely be responsible for the absence of grain boundaries in the SY:DNA-CTMA:TBABF$_4$ films (Figure S4.1, Supporting Information). Despite these well-dispersed ions, the non-polar nature of SY causes a dramatically lower ionic conductivity in the SY:TBABF$_4$ than in SY:DNA-CTMA:TBABF$_4$ blends (Figure 1c).

A very inhomogeneous light output was observed for the reference LECs without DNA-CTMA, using the same stack under same operational conditions as with the polyelectrolyte (Figure S5.2a–d, Supporting Information). The LIV characteristics of the reference devices exhibited turn-on voltages of 6.2–11 V, that is, about 2 V higher than the LECs comprising DNA-CTMA SPEs in the active layer (Figure 3d). Also, the maximum luminance intensity was lower and ranged within 1600–1800 cd cm^{-2} (Figure S5.2d, Supporting Information). The (5:0:1) device with the lowest turn-on voltage of $V_{on} = 6.2$ V exhibited a maximum luminance L_{max} of only 244 cd m^{-2} at 8 V, which comprises a lower performance compared to the (5:1:1) LEC with DNA-CTMA with $V_{on} = 3.45 \pm 0.07$ V and $L_{max} = 1717 \pm 311$ cd m^{-2} at 6 V. Clearly, the better ionic dissociation and conductivity in the DNA-CTMA polyelectrolyte improves the LEC device performance.

2.3. DNA-CTMA as a Universal Electrolyte for Arbitrary Emitters

The absence of a reduction and oxidation peak in the cyclic voltammogram of DNA-CTMA (Figure 1b) suggests that it should not only be suitable for emitters with an intermediate bandgap, such as SY, but also for wide bandgap blue-emitting semiconductors. The TBABF$_4$ salt was replaced with its hexylated derivative THABF$_4$, which was described to enable reliable LECs with a variety of emitters in literature.[54,59] In contrast to these investigations and previous electrochemical studies,[60,61] the THABF$_4$ salt and DNA-CTMA:THABF$_4$ SPE did not reveal a larger electrochemical window than TBABF$_4$ salt based SPEs (**Figure 4**a), which might originate in the catalytic properties of the Pt working electrode or electrochemical degradation of the solvent. Nonetheless, the oxidation and reduction onsets of the SPE matches the salt-only solution and is clearly not limited by the DNA-CTMA.
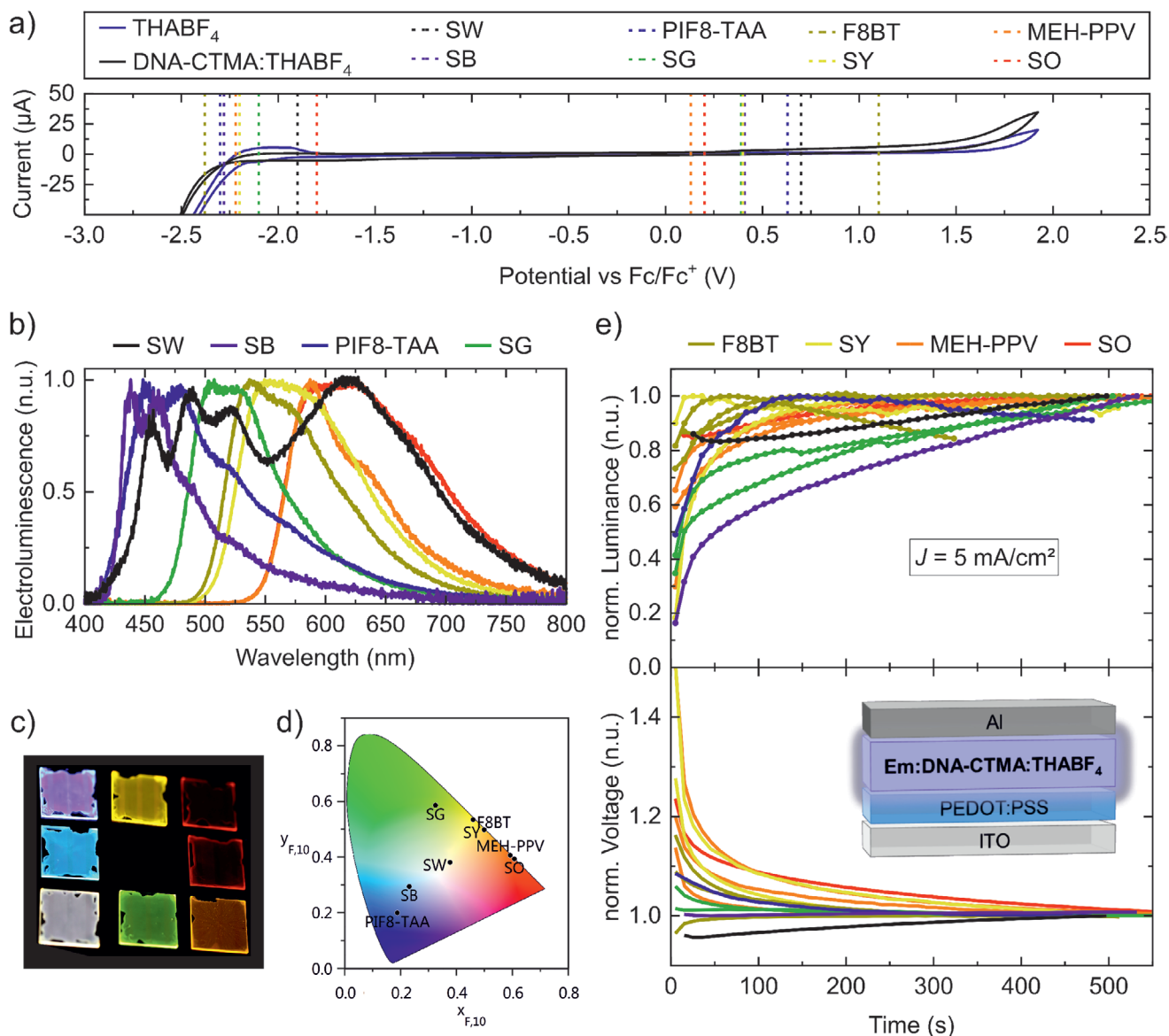
Serving as a blue emitting model compound, a small molecule emitter (TADFa) exhibiting thermally activated delayed fluorescence was blended with the host molecule (PYD2) (see molecular structures in **Scheme 1**). The PYD2:TADFa host:guest system was previously employed in OLEDs,[62] and used for exploring some parameters in DNA-CTMA LECs (details in Section S6, Supporting Information). Using non-alcoholic solvents for the emitter did not impair the LEC performance (Figure S6.1, Supporting Information) and an emitter:DNA-CTMA:THABF$_4$ ratio of (10:1:1) resulted in the highest efficiency without sacrificing the low turn-on voltage (Figures S6.2 and S 6.3, Supporting Information). Clearly, this host:guest system emits solely from the guest and exceeds the efficiency of the individual constituents (Figure S6.4, Supporting Information).

In addition to PYD2:TADFa, we employed nine different polymer emitters to fabricate LECs with the DNA-CTMA:THABF$_4$ SPE. The polymer classes involve poly(phenylene-vinylenes) (super orange "SO," MEH-PPV, "SY"), fluorenes (F8BT, PFO, PIF8-TAA), spirobifluorenes (super blue "SB"), a mix of many copolymerized moieties (super white "SW") or are unknown (super green "SG") (Scheme 1). Eight emitters of this pool, namely SW,[63,64] SB,[63,65] PIF8-TAA,[66–68] SG,[63,69,70] F8BT,[63,71–76] SY,[25,49,63,77] MEH-PPV,[78] and SO[79] exhibit a deeper LUMO than −2.55 eV and shallower HOMO than −6.3 eV (Table S7.1 and Figure S7.1, Supporting Information). Hence, they lie within the electrochemical stability window of DNA-CTMA:THABF$_4$ (Figure 4a). In contrast, the LUMOs of PFO[63,75,76,80,81] and PYD2:TADFa[62] exceed the reduction onset of the SPE, predicting an electrochemically unstable LEC performance (Figure S7.4a, Supporting Information).

Fully optimizing the active blend for each individual of these chemically very different emitter compounds with regard to choice of solvent, ratio of components and thickness of the layer exceeds the scope of this report. Hence, a suitable non-alcoholic solvent was used for each emitter (Table S7.2, Supporting Information) and the emitter:DNA-CTMA:THABF$_4$ ratio was fixed to (10:1:1). The high salt content should minimize the intrinsically large turn-on voltage for these large bandgap emitters. PIF8-TAA, PFO, F8BT, SY, and MEH-PPV show no signs of phase separation, despite using a solvent that does not dissolve DNA-CTMA (Figure S7.2, Supporting Information). The active layer blends of SO and PYD2:TADFa exhibit minor phase separation of below 1 µm between emitter-rich and emitter-poor phases. Larger inhomogeneities of around 2 µm can be observed with SG, SB, and SW. With knowledge of the exact composition (backbone and side-chains) of these three polymers, thorough optimization of the solvent and emitter to electrolyte ratio surely could create better interphase mixing and homogeneous active layers.

The LECs with DNA-CTMA and the eight electrochemically stable active materials emitted light ranging from 425 to 700 nm (Figure 4b). The electroluminescence matches the photoluminescence of the active layers (Figure 4c). This plethora of emitters covers the majority of the CIE chromaticity diagram with red, green, blue, and white colored electroluminescence (Figure 4d).

A key step in the fabrication of reliable LEC devices was employing an aluminum cathode and an ITO/PEDOT:PSS
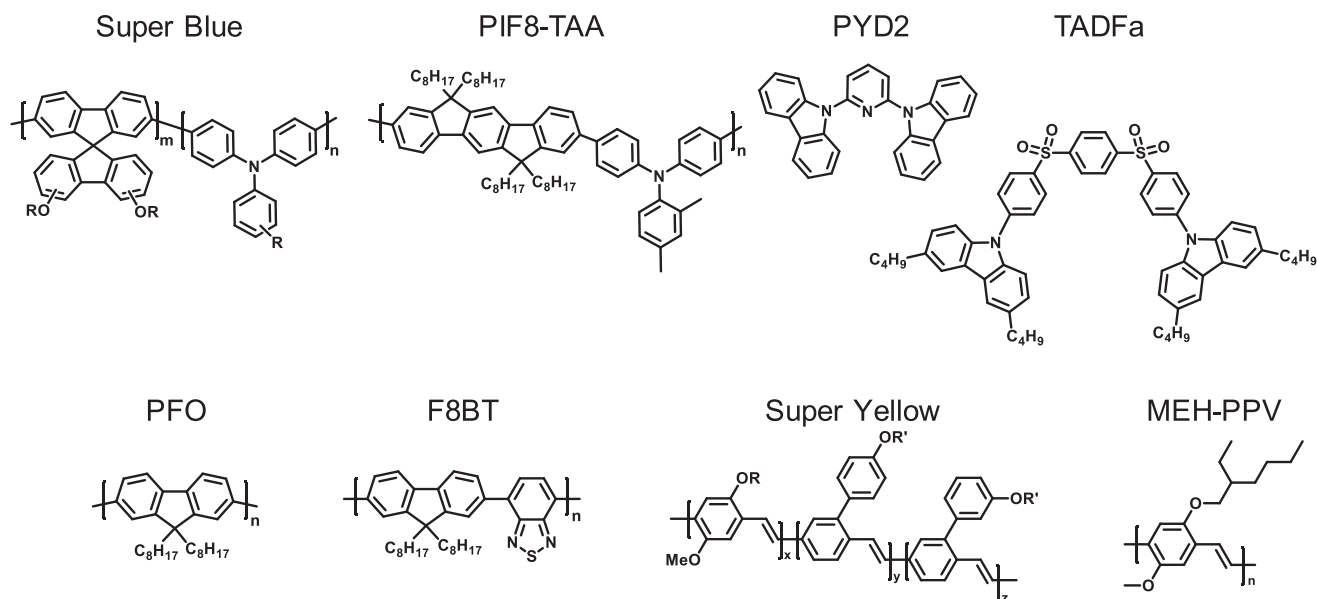
**ADVANCED
SCIENCE NEWS**

www.advancedsciencenews.com

**ADVANCED
SUSTAINABLE
SYSTEMS**

www.advsustainsys.com

Figure 4. Emitter:DNA-CTMA:THABF$_4$ LECs with eight different emitters. a) Cyclic voltammograms of THABF$_4$, DNA-CTMA, and the DNA-CTMA:THABF$_4$ (1:1) blend. The dashed lines mark the reduction and oxidation onsets of the eight emitters. Solvent: acetonitrile, scan rate: 0.05 V s^{-1}. b) Electroluminescence spectra. c) Photograph of eight active layers under UV light. d) CIE chromaticity diagram of the LECs' electroluminescence. e) Steady-state characteristics at 5 mA cm^{-2}. Inset (e): Device architecture. All samples had a w/w ratio of (10:1:1).

anode to achieve reliable electron injection and reduce shorts, especially for green and blue emitters (Figure 4d inset). In steady-state operation at constant current (Figure 4e), their luminance increases asymptotically over time, confirming a stable operation as predicted by cyclic voltammetry (see Figure S7.3, Supporting Information for the graphs of every single material). The turn-on voltages, as derived from the luminance-voltage sweep (Figure S7.3b, Supporting Information), rise from red to blue emitters as expected for an increasing HOMO-LUMO gap (**Table 2**). The highest luminance values were achieved with SY and F8BT emitters. Consequently, these two emitters also produced the highest efficiency (Figure S7.2c, Supporting Information). The progression of the steady-state efficiencies confirms the efficiency trend of the voltage-sweeps. The lower

performance of the SY LECs in Table 2 compared to Table 1 originates in the use of anisole instead of chloroform:butanol, which might enhance the phase separation from the electrolyte on a nanoscale, as well as using different SY batches.

The performance of the blue-emitting PFO and PYD2:TADFa (Figure S7.4b, Supporting Information) draws a contrary picture to the previously discussed eight emitters. Despite maintaining a stable voltage during operation at constant current, the decreasing luminance over time indicates immediate degradation (Figure S7.4c, Supporting Information), likely due to electrochemical degeneration of the DNA-CTMA:THABF$_4$ electrolyte as indicated by the cyclic voltammogram. Hence, the bright and efficient emission of PFO in a voltage sweep and steady-state mode cannot be regarded reliable over time

**ADVANCED
SCIENCE NEWS**
www.advancedsciencenews.com

**ADVANCED
SUSTAINABLE
SYSTEMS**
www.advsustainsys.com

Scheme 1. Molecular structure of Super Blue (SB), PIF8-TAA, PYD2, TADFa, PFO, F8BT, Super Yellow (SY), and MEH-PPV.

(Figure S7.4d,e, Supporting Information). Nonetheless, the successful combination of a DNA-CTMA electrolyte with such a chemically and spectrally large variety of emitters in LECs highlights the versatility of DNA-CTMA electrolytes due to its high reduction and oxidation potentials.

3. Summary and Conclusion

In this work, we have demonstrated the suitability of the natural biopolymer derivative DNA-CTMA as a SPE for LECs. To this end, the modification of DNA with the lipid surfactant CTMA proved to be crucial in order to enable processing in organic solvents and avoid the degradation related to water-based solutions. A thorough analysis of the microstructural evolution upon the addition of an organic salt revealed structure–property relationships between surface morphology, impedance spectra, and ionic conductivity. The inhomogeneous morphology and the salt aggregation in the films decreased the bulk ionic

Table 2. Device characteristics of emitter:DNA-CTMA:THABF$_4$ LECs.

Emitter	V_{on}[a] [V]	L_{max}[b] [cd m^{-2}]	Eff$_{max}$[c] [cd A^{-1}]	L_{steady}[d] [cd m^{-2}]	Eff$_{steady}$[e] [cd A^{-1}]
SO	2.65	100	0.14	7.9	0.16
MEH-PPV	3.35 ± 0.05	211	0.08	3.2 ± 2.2	0.06 ± 0.04
SY	4.29 ± 0.76	474	0.22	8.7 ± 1.7	0.17 ± 0.03
F8BT	4.81 ± 0.26	476	0.27	4.5 ± 3.1	0.09 ± 0.07
SG	7.67 ± 0.06	16	0.04	1.8 ± 0.04	0.04 ± 0.001
PIF8-TAA	4.00 ± 0.20	328	0.19	0.5	0.009
SB	7.00 ± 0.14	344	0.16	0.8 ± 0.9	0.02 ± 0.02
SW	6.06 ± 0.03	96	0.05	1.7 ± 1.5	0.03 ± 0.03

[a] Turn-on voltage at 1 cd m^{-2}; [b] Maximum luminance; [c] Maximum current efficiency at LIV sweep; [d] Luminance; [e] Current density at steady state at 5 mA cm^{-2}.

conductivity of the SPE. However, blending with a well-studied yellow emissive polymer homogenized the micro- and nanostructure. The performance of the resulting LECs does not surpass commonly applied synthetic ion-solvating polymers, while the additional merit of biodegradability is obvious. The composition of the emitter, DNA-CTMA, and salt needs to be tuned to the intended application of the LEC, focusing either on maximizing the efficiency, lifetime, or luminance.

In order to highlight the outstanding electrochemical stability of DNA-CTMA and its versatility as an ion-solvating polymer, we employed eight different polymer emitters, enabling LEC devices with electroluminescent emission across the entire visible spectrum. The emission remained stable as long as the injection levels are situated within the electrochemical stability window of the SPE. The high reduction onset of DNA-CTMA enables the combination not only with commonly employed red and yellow but also with green and blue emitters having a high LUMO. In essence, the good ion-conducting properties and a high electrochemical stability window make DNA-CTMA an almost universal SPE for visible light emission in LECs.

Looking into the future, the development of high performance LECs based on naturally sourced materials will still need to be accompanied by the development of biodegradable and efficient semiconducting emitters and the utilization of cost- and material-efficient production processes such as printing technologies. Surely, the simplicity and advantages of LECs will help them contribute to the necessary research efforts in the fabrication of more eco- and bio-friendly electronics.

4. Experimental Section

Materials: DNA-CTMA was prepared by modifying DNA as described in Section S2, Supporting Information. TBABF$_4$ salt (tetrabutylammonium tetrafluoroborate), THABF$_4$ salt (tetrahexylammonium tetrafluoroborate), F8BT polymer (poly(9,9-dioctylfluorene-*alt*-benzothiadiazole), M_n = 10–20 kDa), MEH-PPV

**ADVANCED
SCIENCE NEWS**

www.advancedsciencenews.com

**ADVANCED
SUSTAINABLE
SYSTEMS**

www.advsustainsys.com

polymer (poly(2-methoxy-5-(2-ethylhexyloxy)-1,4-phenylenevinylene), M_n = 70–100 kDa), PFO polymer (poly(9,9-dioctylfluoren-2,7-diyl)), and PYD2 molecule (2,6-Bis(9H-carbazol-9-yl)pyridine) were purchased from Sigma-Aldrich. SB polymer (SB, Polymer Blue SPB-02T), SG polymer (SG, Polymer Green SPG-01T-L05), SO polymer (SO PDO-123), SW polymer (SW, Polymer White SPW-111-020), SY polymer (SY PYD-132), and PIF8-TAA polymer (Polyindenofluorene-8-triarylamine, Polytos, M_w = 180 kDa) were purchased from Merck KGaA. TADFa molecule (1,4-bis{[4-(3,6-di-n-butyl)carbazolylphenyl]sulfonyl}-benzene) was synthesized as previously described.[62] PEDOT:PSS (VAPI 4083) was obtained from Heraeus.

Cyclic Voltammetry: A VERSASTAT 3 potentiostat (Princeton Applied Research) or an Autolab PGSTAT potentiostat was combined with a 3-electrode system (Pt working electrode with a dropcasted film, Pt/Ti counter electrode, and Ag wire pseudo-reference electrode). Acetonitrile containing 0.1 M tetrabutylammonium hexafluorophosphate (TBAPF$_6$, >99%, Sigma-Aldrich, for SY and DNA-CTMA) or 0.1 M TBABF$_4$ (for DNA-CTMA:TBABF$_4$ and SY:DNA-CTMA:TBABF$_4$) or 0.1 M THABF$_4$ (for DNA-CTMA:THABF$_4$ and SY:DNA-CTMA:THABF$_4$) was used as the supporting electrolyte. A small amount of ferrocene (di(cyclopentadienyl) iron, >98%, Sigma-Aldrich) was used as an internal reference redox system for each sample. All CV measurements were performed under N$_2$ atmosphere at a scan rate of 0.05 V s^{-1}. The oxidation and reduction onsets $V_{ox/red}$ were converted to HOMOs and LUMOs via $E_{HOMO/LUMO}$ = $-$ ($V_{ox/red}$ + 4.8).[82–84]

Impedance Spectroscopy: Characterization and modeling are detailed in Section S3, Supporting Information.

Profilometry: Thickness measurements were performed using a Veeco profilometer.

White Light Interferometry: Samples were deposited from the same solutions as the LECs and measured with a Sensofar PLu Neox White Light 3D Interferometer using 10× magnification objective with the monochromatic illumination in the phase shifting interferometry measurement mode. The root-mean-square roughness values were obtained for the entire field of view.

Microscopy: A Nikon Eclipse 80i microscope was used in bright field or photoluminescence mode. The latter employed one of these filter cubes: DAPI (excitation 352–402 nm, dichroic mirror 409 nm, emission 417–477 nm), FITC (exc. 465–495 nm, d.m. 505 nm, em. 515–555 nm), and TxRed (exc.542–576 nm, d.m. 587 nm, em. 595–665 nm).

Atomic Force Microscopy: A DME DualScope 95-50 atomic force microscope was used in tapping mode.

Device Fabrication for SY:DNA-CTMA:TBABF$_4$ LECs: SY, DNA-CTMA, and the TBABF$_4$ were dissolved separately in a v/v 2:1 mix of chloroform:butanol at the concentration of 2.5 g L^{-1}. DNA-CTMA solution was filtered through a 0.45 µm pore sized PTFE filter to remove residual particles after the modification process. All solutions were mixed at different w/w ratios, that is, v/v ratios as a result of equal concentration. Solutions were spin-coated in ambient atmosphere onto ITO at 5000 rpm for 90 s, forming film thicknesses at the range of 70–75 nm. Finally, 100 nm thick Ag top contacts were thermally evaporated through a shadow mask to define the active pixel area of the device (0.24 cm^2).

Device Fabrication for Emitter:DNA-CTMA:THABF$_4$ LECs: DNA-CTMA and THABF$_4$ were dissolved separately in a 2:1 mix of chloroform:butanol at the concentration of 10 g L^{-1}. DNA-CTMA solution was filtered through a 5 µm pore sized PTFE filter. The salt was filtered through a 0.2 µm PTFE or PVDF filter. Since not all of the ten emitter materials were soluble in the 2:1 mixture of CF:BuOH (used for SY:DNA-CTMA:TBABF$_4$ LECs), each emitter was dissolved in a suitable non-alcoholic organic solvent. The respective solvents and concentrations are listed in Table S7.2, Supporting Information. Of these, the emitting polymer solutions were not filtered and the PYD2:TADFa solution was filtered through a 0.2 µm PVDF filter. All solutions were mixed at a w/w ratio of (10:1:1). Pre-patterned ITO substrates were covered with 0.45 µm PVDF-filtered PEDOT:PSS by spin-coating at 4000 rpm, 1000 rpm s^{-1}, 60 s, and subsequently annealed at 140 °C for 10 min, yielding a 33 ± 3 nm thick film. The mixed emitter:DNA-CTMA:THABF$_4$ solutions were then spin-coated in N$_2$ atmosphere onto the PEDOT:PSS layer at 800 rpm for 120 s and annealed at 60 °C (to avoid any decomposition of the DNA-CTMA) for 30 min. The film thicknesses are compiled in Table S7.2, Supporting Information. A 100 nm layer of Al was evaporated as a top electrode, patterned by a shadow-mask.

LEC Characterization: The optoelectrical characterization of all devices was performed using a calibrated BOTEST system in N$_2$ atmosphere, or air after encapsulation. The LIV sweeps were conducted at a speed of 0.1 V s^{-1}. The steady-state and lifetime measurements had a sampling interval of 10 s. The pixels were filmed in operation with a DNT DigiMicro camera. The electroluminescence spectra were recorded using an Ocean Optics spectrophotometer. The calculations and figures related to CIE chromaticity coordinates were done with the SpectrAsis or Osram Color Calculator software.

Supporting Information

Supporting Information is available from the Wiley Online Library or from the author.

Conflict of Interest

The authors declare no conflict of interest.

[1] M. Irimia-Vladu, *Chem. Soc. Rev.* **2014**, *43*, 588.

[2] E. Fresta, V. Fernández-Luna, P. B. Coto, R. D. Costa, *Adv. Funct. Mater.* **2018**, *28*, 1707011.

[3] V. R. Feig, H. Tran, Z. Bao, *ACS Cent. Sci.* **2018**, *4*, 337.

[4] M. Irimia-Vladu, E. D. Glowacki, N. S. Sariciftci, S. Bauer, *Green Materials for Electronics*, Wiley-VCH, Weinheim, Germany **2017**.

[5] T. Someya, Z. Bao, G. G. Malliaras, *Nature* **2016**, *540*, 379.

[6] A. J. Morfa, T. Rödlmeier, N. Jürgensen, S. Stolz, G. Hernandez-Sosa, *Cellulose* **2016**, *23*, 3809.

[7] Q. Sun, B. Qian, K. Uto, J. Chen, X. Liu, T. Minari, *Biosens. Bioelectron.* **2018**, *119*, 237.

[8] A. Chortos, J. Liu, Z. Bao, *Nat. Mater.* **2016**, *15*, 937.

[9] M. Amjadi, K.-U. Kyung, I. Park, M. Sitti, *Adv. Funct. Mater.* **2016**, *26*, 1678.

[10] T. Q. Trung, N.-E. Lee, *Adv. Mater.* **2016**, *28*, 4338.

**ADVANCED
SCIENCE NEWS**

www.advancedsciencenews.com

**ADVANCED
SUSTAINABLE
SYSTEMS**

www.advsustainsys.com

[11] M. J. Tan, C. Owh, P. L. Chee, A. K. K. Kyaw, D. Kai, X. J. Loh, *J. Mater. Chem. C* **2016**, *4*, 5531.

[12] P. Modak, in *Towards a Green Economy: Pathways to Sustainable Development and Poverty Eradication*, United Nations Environment Programme, Nairobi **2011**, pp. 227–330.

[13] M. Heacock, C. B. Kelly, K. A. Asante, L. S. Birnbaum, Å. L. Bergman, M.-N. Bruné, I. Buka, D. O. Carpenter, A. Chen, X. Huo, M. Kamel, P. J. Landrigan, F. Magalini, F. Diaz-Barriga, M. Neira, M. Omar, A. Pascale, M. Ruchirawat, L. Sly, P. D. Sly, M. van den Berg, W. A. Suk, *Environ. Health Perspect.* **2016**, *124*, 550.

[14] S.-K. Kang, J. Koo, Y. K. Lee, J. A. Rogers, *Acc. Chem. Res.* **2018**, *51*, 988.

[15] E. Kim, Y. Xiong, Y. Cheng, H.-C. Wu, Y. Liu, B. Morrow, H. Ben-Yoav, R. Ghodssi, G. Rubloff, J. Shen, W. Bentley, X. Shi, G. Payne, *Polymers* **2015**, *7*, 1.

[16] Q. Pei, G. Yu, C. Zhang, Y. Yang, A. J. Heeger, *Science* **1995**, *269*, 1086.

[17] *Light-Emitting Electrochemical Cells: Concepts, Advances and Challenges* (Ed: R. D. Costa), Springer, Berlin **2017**.

[18] J. Zimmermann, L. Porcarelli, T. Rödlmeier, A. Sanchez-Sanchez, D. Mecerreyes, G. Hernandez-Sosa, *Adv. Funct. Mater.* **2018**, *28*, 1705795.

[19] J. Zimmermann, S. Schlisske, M. Held, J.-N. Tisserant, L. Porcarelli, A. Sanchez-Sanchez, D. Mecerreyes, G. Hernandez-Sosa, *Adv. Mater. Technol.* **2019**, *4*, 1800641.

[20] N. Jürgensen, J. Zimmermann, A. J. Morfa, G. Hernandez-Sosa, *Sci. Rep.* **2016**, *6*, 36643.

[21] J. Zimmermann, N. Jürgensen, A. J. Morfa, B. Wang, S. Tekoglu, G. Hernandez-Sosa, *ACS Sustainable Chem. Eng.* **2016**, *4*, 7050.

[22] Y. Cao, G. Yu, A. J. Heeger, C. Y. Yang, *Appl. Phys. Lett.* **1996**, *68*, 3218.

[23] P. Matyba, M. R. Andersson, L. Edman, *Org. Electron.* **2008**, *9*, 699.

[24] S. Tang, L. Edman, *J. Phys. Chem. Lett.* **2010**, *1*, 2727.

[25] S. Tang, J. Mindemark, C. M. G. Araujo, D. Brandell, L. Edman, *Chem. Mater.* **2014**, *26*, 5083.

[26] J. Mindemark, S. Tang, J. Wang, N. Kaihovirta, D. Brandell, L. Edman, *Chem. Mater.* **2016**, *28*, 2618.

[27] J. Mindemark, L. Edman, *J. Mater. Chem. C* **2016**, *4*, 420.

[28] G. S. Manning, *Q. Rev. Biophys.* **1978**, *11*, 179.

[29] M. Mindroiu, A.-M. Manea, I. Rau, J. G. Grote, H. C. Oliveira, A. Pawlicka, F. Kajzar, in *ROMOPTO 2012: Tenth Conference on Optics: Micro- to Nanophotonics III* (Ed: V. I. Vlad), SPIE, Bellingham, WA **2013**, p. 888202.

[30] J. G. Grote, J. A. Hagen, J. S. Zetts, R. L. Nelson, D. E. Diggs, M. O. Stone, P. P. Yaney, E. Heckman, C. Zhang, W. H. Steier, A. K.-Y. Jen, L. R. Dalton, N. Ogata, M. J. Curley, S. J. Clarson, F. K. Hopkins, *J. Phys. Chem. B* **2004**, *108*, 8584.

[31] K. Tanaka, Y. Okahata, *J. Am. Chem. Soc.* **1996**, *118*, 10679.

[32] D. Wanapun, V. J. Hall, N. J. Begue, J. G. Grote, G. J. Simpson, *ChemPhysChem* **2009**, *10*, 2674.

[33] R. Khazaeinezhad, S. Hosseinzadeh Kassani, B. Paulson, H. Jeong, J. Gwak, F. Rotermund, D.-I. Yeom, K. Oh, *Sci. Rep.* **2017**, *7*, 41480.

[34] Z. Yu, W. Li, J. A. Hagen, Y. Zhou, D. Klotzkin, J. G. Grote, A. J. Steckl, *Appl. Opt.* **2007**, *46*, 1507.

[35] B. Singh, N. S. Sariciftci, J. G. Grote, F. K. Hopkins, *J. Appl. Phys.* **2006**, *100*, 024514.

[36] C. Yumusak, T. B. Singh, N. S. Sariciftci, J. G. Grote, *Appl. Phys. Lett.* **2009**, *95*, 263304.

[37] P. Stadler, K. Oppelt, T. B. Singh, J. G. Grote, R. Schwödiauer, S. Bauer, H. Piglmayer-Brezina, D. Bäuerle, N. S. Sariciftci, *Org. Electron.* **2007**, *8*, 648.

[38] J. A. Hagen, W. Li, A. J. Steckl, J. G. Grote, *Appl. Phys. Lett.* **2006**, *88*, 171109.

[39] R. Grykien, B. Luszczynska, I. Glowacki, F. Kajzar, I. Rau, *Mol. Cryst. Liq. Cryst.* **2014**, *604*, 213.

[40] Q. Sun, G. Subramanyam, L. Dai, M. Check, A. Campbell, R. Naik, J. Grote, Y. Wang, *ACS Nano* **2009**, *3*, 737.

[41] K. Nakamura, T. Ishikawa, D. Nishioka, T. Ushikubo, N. Kobayashi, *Appl. Phys. Lett.* **2010**, *97*, 193301.

[42] R. Grykien, B. Luszczynska, I. Glowacki, J. Ulanski, F. Kajzar, R. Zgarian, I. Rau, *Opt. Mater.* **2014**, *36*, 1027.

[43] S. Tsuneyasu, R. Takahashi, H. Minami, K. Nakamura, N. Kobayashi, *Sci. Rep.* **2017**, *7*, 8525.

[44] A. Pawlicka, A. Firmino, D. Vieira, F. Sentanin, J. G. Grote, F. Kajzar, in *Optical Materials in Defence Systems Technology VI* (Eds: J. G. Grote, F. Kajzar, R. Zamboni), SPIE, Bellingham, WA **2009**, p. 74870J.

[45] A. Pawlicka, F. Sentanin, A. Firmino, J. G. Grote, F. Kajzar, I. Rau, *Synth. Met.* **2011**, *161*, 2329.

[46] J. Kumar, F. Ouchen, D. A. Smarra, G. Subramanyam, J. G. Grote, in *Nanobiosystems: Processing, Characterization, and Applications VIII* (Eds: N. Kobayashi, F. Ouchen, I. Rau), SPIE, Bellingham, WA **2015**, p. 95570A.

[47] C. C. Jayme, J. Kanicki, F. Kajzar, A. F. Nogueira, A. Pawlicka, *Mol. Cryst. Liq. Cryst.* **2016**, *627*, 38.

[48] A. Ghosh, M. Bansal, *Acta Crystallogr., Sect. D: Struct. Biol.* **2003**, *59*, 620.

[49] G. Hernandez-Sosa, S. Tekoglu, S. Stolz, R. Eckstein, C. Teusch, J. Trapp, U. Lemmer, M. Hamburger, N. Mechau, *Adv. Mater.* **2014**, *26*, 3235.

[50] I. Khimji, J. Shin, J. Liu, *Chem. Commun.* **2013**, *49*, 1306.

[51] J. Gao, Y. Li, G. Yu, A. J. Heeger, *J. Appl. Phys.* **1999**, *86*, 4594.

[52] G. Hernandez-Sosa, R. Eckstein, S. Tekoglu, T. Becker, F. Mathies, U. Lemmer, N. Mechau, *Org. Electron.* **2013**, *14*, 2223.

[53] S. Tang, W.-Y. Tan, X.-H. Zhu, L. Edman, *Chem. Commun.* **2013**, *49*, 4926.

[54] S. Tang, A. Sandström, P. Lundberg, T. Lanz, C. Larsen, S. van Reenen, M. Kemerink, L. Edman, *Nat. Commun.* **2017**, *8*, 1190.

[55] J. Fang, P. Matyba, N. D. Robinson, L. Edman, *J. Am. Chem. Soc.* **2008**, *130*, 4562.

[56] S. van Reenen, P. Matyba, A. Dzwilewski, R. A. J. Janssen, L. Edman, M. Kemerink, *Adv. Funct. Mater.* **2011**, *21*, 1795.

[57] D. Tordera, J. Frey, D. Vonlanthen, E. Constable, A. Pertegás, E. Ortí, H. J. Bolink, E. Baranoff, M. K. Nazeeruddin, *Adv. Energy Mater.* **2013**, *3*, 1338.

[58] S. van Reenen, R. A. J. Janssen, M. Kemerink, *Adv. Funct. Mater.* **2015**, *3*, 3066.

[59] W. Xiong, S. Tang, P. Murto, W. Zhu, L. Edman, E. Wang, *Adv. Opt. Mater.* **2019**, *7*, 1900280.

[60] S.-F. Zhao, M. Horne, A. M. Bond, J. Zhang, *J. Phys. Chem. C* **2016**, *120*, 23989.

[61] M. Ue, *J. Electrochem. Soc.* **1994**, *141*, 2989.

[62] N. Jürgensen, A. Kretzschmar, S. Höfle, J. Freudenberg, U. H. F. Bunz, G. Hernandez-Sosa, *Chem. Mater.* **2017**, *29*, 9154.

[63] N. Bolse, R. Eckstein, M. Schend, A. Habermehl, C. Eschenbaum, G. Hernandez-Sosa, U. Lemmer, *Flexible Printed Electron.* **2017**, *2*, 024001.

[64] M. A. Mohd Sarjidan, H. A. Mohd Mokhtar, W. H. Abd, *J. Lumin.* **2015**, *159*, 134.

[65] Y. Y. Kim, W. J. Hyun, K. H. Park, Y. G. Lee, J. Lee, O. O. Park, *J. Mater. Chem. C* **2016**, *4*, 10445.

[66] M. Pietsch, T. Rödlmeier, S. Schlisske, J. Zimmermann, C. Romero-Nieto, G. Hernandez-Sosa, *J. Mater. Chem. C* **2019**, *7*, 7121.

[67] S. Ryu, J. H. Noh, N. J. Jeon, Y. Chan Kim, W. S. Yang, J. Seo, S. I. Seok, *Energy Environ. Sci.* **2014**, *7*, 2614.

[68] W. Zhang, J. Smith, R. Hamilton, M. Heeney, J. Kirkpatrick, K. Song, S. E. Watkins, T. Anthopoulos, I. McCulloch, *J. Am. Chem. Soc.* **2009**, *131*, 10814.

[69] J. Ha, J. Park, J. Ha, D. Kim, S. Chung, C. Lee, Y. Hong, *Org. Electron.* **2015**, *19*, 147.

[70] J. H. Youn, Y. I. Lee, H. T. Moon, S. J. Baek, J. Jang, *Soc. Inf. Disp. Int. Symp. Dig. Tech. Pap.* **2011**, *42*, 1729.

[71] M. K. Fung, S. W. Tong, S. L. Lai, S. N. Bao, C. S. Lee, W. W. Wu, M. Inbasekaran, J. J. O'Brien, S. Y. Liu, S. T. Lee, *J. Appl. Phys.* **2003**, *94*, 2686.

[72] L.-L. Chua, J. Zaumseil, J.-F. Chang, E. C.-W. Ou, P. K.-H. Ho, H. Sirringhaus, R. H. Friend, *Nature* **2005**, *434*, 194.

[73] A. C. Morteani, A. S. Dhoot, J.-S. Kim, C. Silva, N. C. Greenham, C. Murphy, E. Moons, S. Ciná, J. H. Burroughes, R. H. Friend, *Adv. Mater.* **2003**, *15*, 1708.

[74] M. C. Gwinner, Y. Vaynzof, K. K. Banger, P. K. H. Ho, R. H. Friend, H. Sirringhaus, *Adv. Funct. Mater.* **2010**, *20*, 3457.

[75] J. Morgado, A. Charas, J. A. Fernandes, I. S. Gonçalves, L. D. Carlos, L. Alcácer, *J. Phys. D: Appl. Phys.* **2006**, *39*, 3582.

[76] J. Sun Park, B. Ram Lee, E. Jeong, H.-J. Lee, J. Min Lee, J.-S. Kim, J. Young Kim, H. Young Woo, S. Ouk Kim, M. Hoon Song, *Appl. Phys. Lett.* **2011**, *99*, 163305.

[77] M. Zhang, S. Höfle, J. Czolk, A. Mertens, A. Colsmann, *Nanoscale* **2015**, *7*, 20009.

[78] L. F. Santos, R. C. Faria, L. Gaffo, L. M. Carvalho, R. M. Faria, D. Gonçalves, *Electrochim. Acta* **2007**, *52*, 4299.

[79] J. Zimmermann, *Gedruckte Elektrochemische Leuchtzellen auf Basis von Biologisch Kompatiblen und Biologisch Abbaubaren Materialien*, Karlsruher, Karlsruhe, Germany **2019**.

[80] S. Janietz, D. D. C. Bradley, M. Grell, C. Giebeler, M. Inbasekaran, E. P. Woo, *Appl. Phys. Lett.* **1998**, *73*, 2453.

[81] G. Latini, L. W. Tan, F. Cacialli, S. R. P. Silva, *Org. Electron.* **2012**, *13*, 992.

[82] B. W. D'Andrade, S. Datta, S. R. Forrest, P. Djurovich, E. Polikaprov, M. E. Thompson, *Org. Electron.* **2005**, *6*, 11.

[83] L. N. Leonat, G. Sbarcea, I. V. Branzoi, *Sci. Bull. - "Politeh." Univ. Bucharest, Ser. B* **2013**, *75*, 111.

[84] C. M. Cardona, W. Li, A. E. Kaifer, D. Stockdale, G. C. Bazan, *Adv. Mater.* **2011**, *23*, 2367.